*Building and Environment*, Vol. 22, No. 2, pp. 129–134, 1987.
Printed in Great Britain.

0360-1323/87 $3.00 + 0.00




# Numerical Modelling of Wind Loading on a Film Clad Greenhouse

E. H. MATHEWS*
J. P. MEYER*

*The reliable prediction of wind loading on film clad greenhouses is essential to their safe and economic design. In this paper the numerical modelling of wind loads on a semicircular greenhouse is discussed. An outline of the numerical model and a detailed discussion of boundary and turbulence modelling are given. Relevant turbulence constants for modelling atmospheric turbulence as well as a special grid generation technique are investigated. A parametric study of the effect of Reynolds number on the wind loading is also presented. Predicted wind loads are successfully compared with published full-scale measurements.*

## NOMENCLATURE

| | |
|---|---|
| $B$ | constant |
| $C_p$ | pressure coefficient |
| $C_1, C_2, C_\mu, C_D$ | coefficients in turbulent transport equations |
| div | divergence |
| $h_{ref}$ | reference height (ridge height = 3.1 m) |
| $I$ | turbulence intensity |
| $k$ | turbulent kinetic energy (time averaged) |
| $k_s$ | surface friction coefficient |
| $L$ | length scale of turbulence |
| $P$ | pressure |
| $V$ | velocity (time averaged) |
| $V_{ref}$ | velocity at height $h_{ref}$ |
| $x$ | $x$-direction (horizontal) |
| $y$ | $y$-direction (vertical) |
| $z$ | turbulence property |

*Greek symbols*

| | |
|---|---|
| $\alpha$ | mean wind speed exponent |
| $\varepsilon$ | dissipation rate of turbulent kinetic energy (time averaged) |
| $\mu$ | effective viscosity (laminar plus turbulent viscosity) |
| $\rho$ | density |
| $\sigma_k, \sigma_\varepsilon$ | coefficients in approximated turbulent transport equations |

*Subscripts*

| | |
|---|---|
| ref | reference |
| t | turbulent |
| $x$ | main flow direction |
| $y$ | perpendicular to main flow direction |
| $z$ | turbulence property ($k$ or $\varepsilon$) |

*Other*

| | |
|---|---|
| $\nabla$ | del operator |
| D( )/Dt | substantial derivative; that is, differentiation following the motion of a fluid particle |
| $\bar{\ }$ | vector quantity |

* Department of Mechanical Engineering, University of Pretoria, Pretoria 0002, South Africa.

## 1. INTRODUCTION

THE USE of plastic film as cladding material for horticultural and agricultural greenhouses has rapidly developed over the past 17 years [1]. Unfortunately, film clad greenhouses are susceptible to wind damage. To ensure not only a safe, but also an economical design, the wind loading on the proposed greenhouse must be reliably predicted at the design stage.

Boundary layer wind tunnels are often employed to acquire the necessary wind loading data. However, many designers do not have access to such tunnels. These tests are also laborious and expensive [2]. It is further difficult to simulate the atmospheric boundary layer and turbulence for complex terrains.

In some cases it may be possible to measure wind loading data on full-scale buildings. Hoxey and co-workers [1, 3, 4] for example did extensive measurements of wind loading on different types of full-scale greenhouses. Unfortunately very few designers have access to the sensitive and expensive monitoring equipment which are needed for such measurements.

Another possibility is to simulate the wind flow and the resulting wind loadings numerically. For many flow cases the numerical solution of the flow equations can produce similar results as the aforementioned procedures, without their disadvantages [5]. It is also very convenient to do parametric studies with computational procedures, as the boundary conditions can easily be changed.

Although numerical modelling of wind loads around buildings could be a useful tool for building designers, relatively little work has been done in this field. Some researchers as Frost and co-workers [6, 7], Yeung and Kot [8] and Wilson and co-workers [2, 9–11] have modelled flow fields around buildings or models of buildings, but few have solved the resulting wind loadings. In some of the papers by Wilson and co-workers [2, 10, 11], predicted wind loading data are given. Only buildings with sharp corners are however

analysed. As wind loads are less dependent on Reynolds number for buildings with sharp corners it was decided to investigate the accuracy of numerically modelled wind loads around a semicircular greenhouse, where loads are dependent on Reynolds number. The modelling of atmospheric turbulence in the proposed procedure is further more accurate than the modelling procedure used by Wilson and co-workers. It is also the aim of this paper to describe a grid generation technique that can be used to generate a boundary fitting solution grid for a non-rectangular obstruction like the greenhouse.

## 2. OUTLINE OF THE MODELLING PROCEDURE

2.1. *Governing differential equations*

The partial differential equations that govern the movement of a viscous fluid are the Navier–Stokes equations and the continuity equation. In the case of incompressible flow the Navier–Stokes equations in vector notation are given by [5],

$$\rho \frac{\mathrm{D}\bar{\mathrm{V}}}{\mathrm{Dt}} = -\mathrm{grad}\, P + \mu \nabla^2 \bar{\mathrm{V}} \tag{1}$$

while the continuity equation in vector notation is given by

$$\mathrm{div}\, \bar{\mathrm{V}} = 0 \tag{2}$$

where D/Dt is the substantial derivative, $\bar{\mathrm{V}}$ the velocity vector, $\rho$ the density, $P$ the pressure and $\mu$ the effective viscosity.

For the simulation of turbulence in the flow, the $k$-$\varepsilon$ turbulent viscosity model is employed. The time-mean partial differential equation for the transport of the turbulence property $z$, where $z$ can denote either $k$ or $\varepsilon$, is given by [12],

$$\rho \frac{\mathrm{D}z}{\mathrm{Dt}} = \mathrm{div}\left[\frac{\mu_t}{\sigma_z}\mathrm{grad}\, z\right] + \left[C_1 \frac{\mu_t}{k}(\mathrm{div}\, \bar{\mathrm{V}})^2 - BC_2 \frac{\rho\varepsilon}{k}\right] \tag{3}$$

where $\mu_t = C_\mu \rho k^2/\varepsilon$ is the turbulent viscosity. If the turbulence property $z$ in equation (3) is the kinetic energy $k$, the value of $C_1$ will be equal to unity while the value of $B$ will equal $1/C_2$. By substituting the dissipation term $\varepsilon$ into equation (3) the transport equation for $\varepsilon$ is found. The value of $B$ will then be unity. The values of the constants $\sigma_\varepsilon$, $\sigma_k$, $C_\mu$, $C_1$ and $C_2$ depend on the particular flow being investigated and may therefore vary for different flow applications. The following set of turbulence constants for the atmospheric boundary layer, proposed by Yeung and Kot [8], was used for the purpose of this study:

$$\sigma_\varepsilon = 1.0, \quad \sigma_k = 1.0, \quad C_1 = 1.54, \quad C_2 = 2.0.$$

Numerical experiments by the authors further showed that a value of $3 \times 10^{-4}$ for the constant $C_\mu$ should be used for atmospheric turbulence.

2.2. *Finite difference equations and solution procedure*

The finite difference equations for the numerical procedure are derived by integrating the partial differential equations over control volumes surrounding a grid point [5]. The proposed method is therefore often referred to as a control volume method [10]. The finite difference equations are derived and solved in a special way. This special procedure is referred to as the SIMPLE (Semi-Implicit Method for Pressure-Linked Equations) procedure. Details of the SIMPLE procedure are widely published [5, 14].

2.3. *Boundary conditions*

2.3.1. *Upstream conditions.* A power law velocity profile is employed to model the approach atmospheric boundary layer flow. The power law is given by [13]

$$V(y)/V_{\mathrm{ref}} = (y/h_{\mathrm{ref}})^\alpha \tag{4}$$

where $V(y)$ is the mean horizontal wind speed component at height $y$ and $V_{\mathrm{ref}}$ is the mean horizontal wind speed at the reference height $h_{\mathrm{ref}}$. The exponent $\alpha$ is the mean wind speed exponent which is dependent on upstream terrain roughness. Values of $\alpha$ for different terrains are widely published [13].

The inflow length scale values for atmospheric longitudinal turbulence $L$ is approximated by the following empirical equation [13]:

$$L(y) = 151(y/10)^\alpha \tag{5}$$

where $L(y)$ is the turbulence length scale in the flow direction at height $y$. This upstream length scale distribution can be described in the numerical model via inflow values for $\varepsilon(y)$. The relationship between $\varepsilon(y)$ and $L(y)$ is defined by the following equation [12]:

$$\varepsilon(y) = [C_D \rho k(y)^{3/2}]/L(y) \tag{6}$$

where $C_D$ is a constant, with value 0.07 for full-scale atmospheric turbulence.

The turbulence intensity $I(y)$ of natural wind at height $y$ at inflow can also be approximated by an empirical equation, which is given by [13]

$$I(y) = (6,7k_s)^{1/2} V_{\mathrm{ref}}/V(y) \tag{7}$$

where $V_{\mathrm{ref}}$ and $V(y)$ are the mean horizontal speeds at heights $h_{\mathrm{ref}}$ and $y$ respectively and where $k_s$ is a surface roughness parameter which is a measure of the surface friction coefficient of the terrain [13]. As the value of $k(y)$ is a measure of turbulence intensity at height $y$, the turbulence intensity can be simulated at inflow by specifying appropriate values for $k(y)$. The relationship between $k(y)$ and $I(y)$ is given by [5]

$$k(y) = 0.5[I(y) \cdot V(y)]^2. \tag{8}$$

2.3.2. *Down- and freestream conditions.* If the freestream boundary is chosen far enough from the obstruction in the flow, it exerts little influence upon the flow inside the solution domain. Care was therefore taken to ensure that the choice of position of the freestream boundary did not influence the solutions. A zero gradient boundary condition was employed for both the pressures and the velocity components parallel to the boundary. No flow was allowed to cross this boundary. At the downstream end of the solution domain, a zero gradient condition was used for all the variables.

2.3.3. *Conditions at solid boundaries.* Both normal and tangential velocity values are set to zero at solid boundaries. The boundary conditions for turbulence

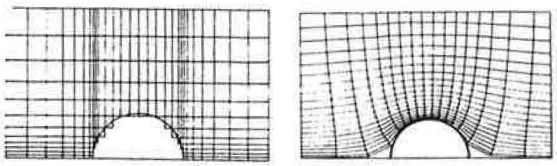

Fig. 1. Orthogonal grid systems. (a) Rectangular. (b) Boundary fitting.

properties near solid walls are, however, more difficult to prescribe. The $k$-$\varepsilon$ model is only valid for fully turbulent flows. A problem therefore arises near a solid boundary where the local Reynolds number becomes very small, resulting in laminar flow. This effect is built into the turbulence model by means of wall functions. The wall functions give a better description of the shear stresses near solid boundaries, resulting in more accurate values for $k$ and for tangential velocities near these boundaries [12].

### 2.4. *Construction of the orthogonal grid*

An orthogonal grid system is needed for the solution of the finite difference equations. A rectangular grid system is usually used (Fig. 1a). The main advantage of this grid is that it is easy to generate. However, the grid cannot accurately describe the boundary of the greenhouse as is shown in Fig. 1a. The orthogonal, boundary fitting grid system given in Fig. 1b is therefore preferable.

A fairly simple procedure is used to generate the boundary fitting grid. A transformed Laplace equation for potential flow is solved in order to establish streamlines for non-viscous flow over the whole flow domain. (The solution of the transformed Laplace equation was described in detail in a previous article [15].) Perpendicular to these streamlines, equipotential lines are calculated and constructed. The complete boundary fitting orthogonal grid is shown in Fig. 1b. This grid is more refined in the vicinity of the solid boundary to ensure an accurate near-wall solution of the Navier–Stokes equations.

Although the grid generation technique was applied to a regular geometry in this paper, it is also applicable to geometries that are not regular. The technique was for example used by the authors to investigate the flow fields over various aeronautical objects with non-regular boundaries. For geometries with many sharp corners it may, however, be better to use a rectangular grid system. Although the authors have not extended the technique to three dimensions, it should be possible to do so.

## 3. NUMERICAL RESULTS AND DISCUSSION

### 3.1. *The example considered*

A semicircular greenhouse was chosen to show the boundary fitting orthogonal grid system as well as to illustrate the numerical model's ability to predict the effect of Reynolds number on the wind loading. Another important reason was that full-scale wind loading measurements were available against which the predicted values could be compared [1]. The full-scale greenhouse had a radius of 3.2 m and a length of 24.4 m. It was slightly recessed into the ground, resulting in a span width of 6.3 m measured at ground level. Measurements were taken at mid-length for transverse flow, as this is usually the more important case in structural design. Because end effects are small at mid-length for this example, a two-dimensional computational approach was assumed sufficient. It was further reasoned that the time-independent Navier Stokes equations would be applicable, as the averaging time for measurements was long, namely 240 s [1].

### 3.2. *Results*

A computer program based on the theory discussed was developed and implemented on a HITACHI PS7/83 mainframe computer. All the solutions generated by the program were obtained with successive refinement of grid size, that is reduction in spacing between grid nodes in the $x$- and $y$-directions. When solutions were observed to be unaffected by further refinements, they were presumed to be grid independent. The grid was more refined in the vicinity of the greenhouse (Fig. 1b). A grid independent solution was found for a $36 \times 40$ grid. Typical calculation times for such a grid were in the order of 500 CPU seconds. The physical dimensions of the solution domain were $60 \times 64$ m.

As full-scale measurements by Hoxey and Richardson [1] were done in open country, corresponding boundary layer profiles for velocity and turbulence properties were simulated in the numerical procedure. Values of 0.15 and $3 \times 10^{-3}$ were respectively used for $\alpha$ and $k_s$ in equations (4), (5) and (7).

A parametric study of the influence of Reynolds number on wind loading was done. The reason for this study was twofold. Firstly to illustrate the dependence of wind loading on Reynolds number for the example considered and secondly to show the versatility of the computational technique. For this particular study, numerical predictions are more advantageous than wind tunnel testing, as it is difficult to simulate full-scale Reynolds numbers in a wind tunnel. Parametric studies of Reynolds number are therefore not really a practical proposition in a wind tunnel. Results of the computational parametric study are shown in Fig. 2. It can be seen that at Reynolds numbers higher than $1 \times 10^6$, the pressure coefficients, therefore wind loading data are independent of Reynolds number. An inflow velocity of more than 5 m/s, measured at the reference height is therefore necessary to ensure that wind loading is independent of Reynolds number.

The numerically predicted and measured [1] mean pressure coefficient distribution for transverse flow and for high Reynolds numbers are shown in Fig. 3. A good agreement between measured and predicted values is observed. One reason for the discrepancy between measured and predicted coefficients at the back of the greenhouse is that it deforms to relieve the pressure forces acting on it. This will of course change the wind loading. The effect of deformation was not taken into account in the computational procedure. However, the predicted pressure coefficients are of sufficient accuracy for structural design purposes. The data were further generated at a fraction of the cost of full-scale data.

Flow separation was predicted at a $x$/span-position of 0.78 while the measured position was 0.67 (see Fig. 3 where the slope of the pressure distribution approaches

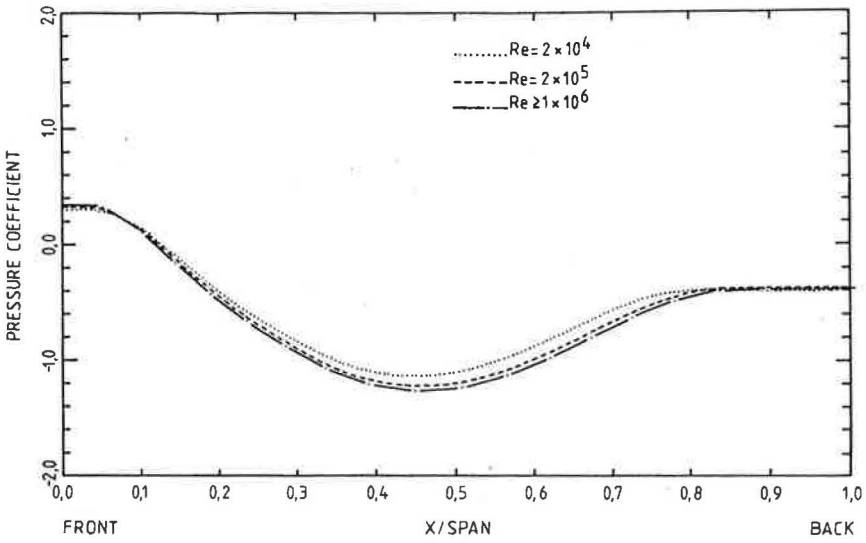


Fig. 2. The influence of Reynolds number (based on $V_{ref}$ and $h_{ref}$) on the wind loading around the greenhouse. The abscissa shows the non-dimensionalized $x$-position on the greenhouse.

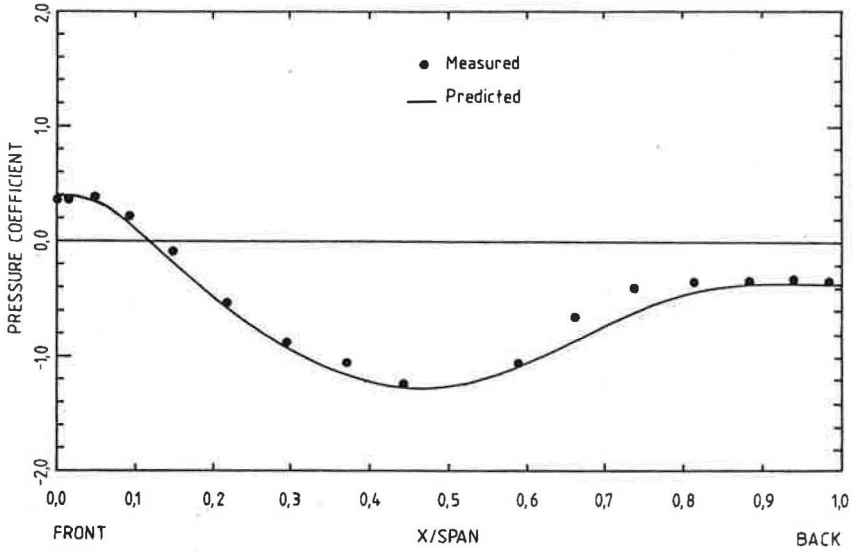


Fig. 3. Measured and predicted pressure coefficient distributions around the greenhouse.

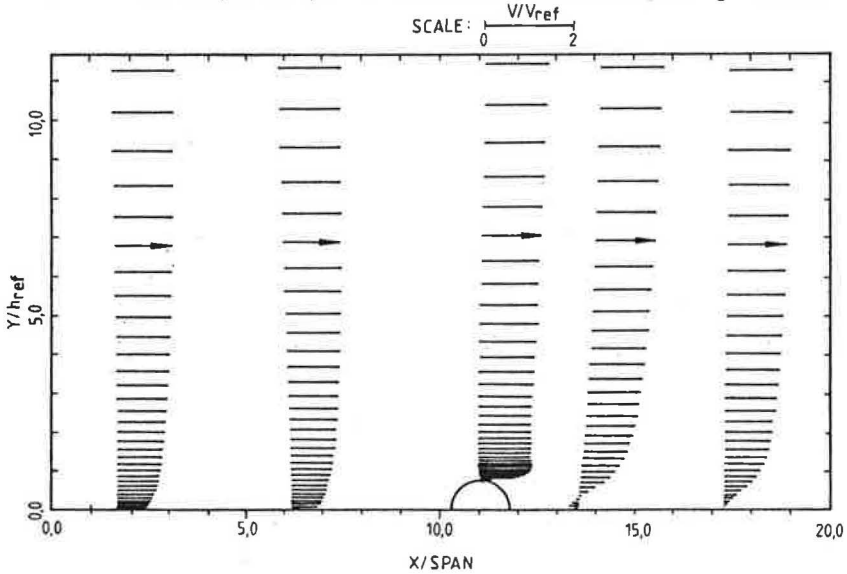


Fig. 4. Predicted horizontal velocities in the flow domain.

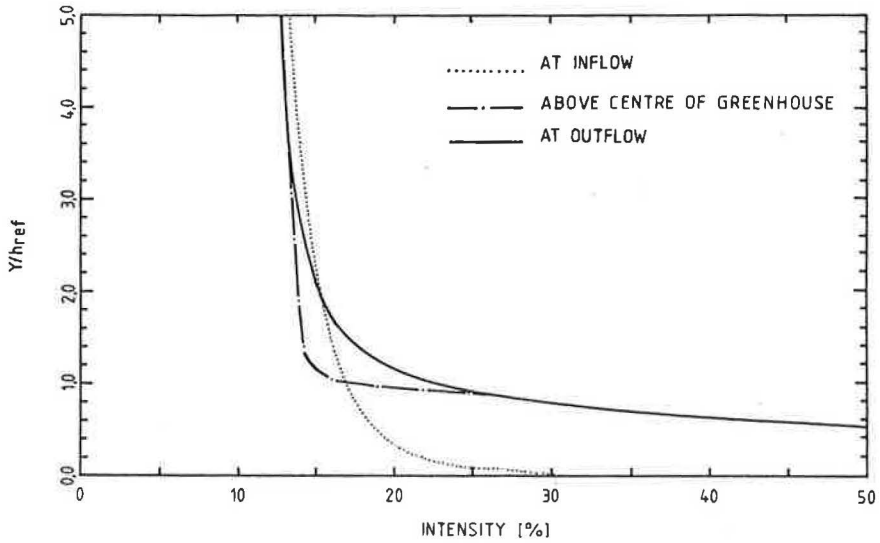


Fig. 5. Predicted turbulence intensities ($I$) at different positions in the flow domain.

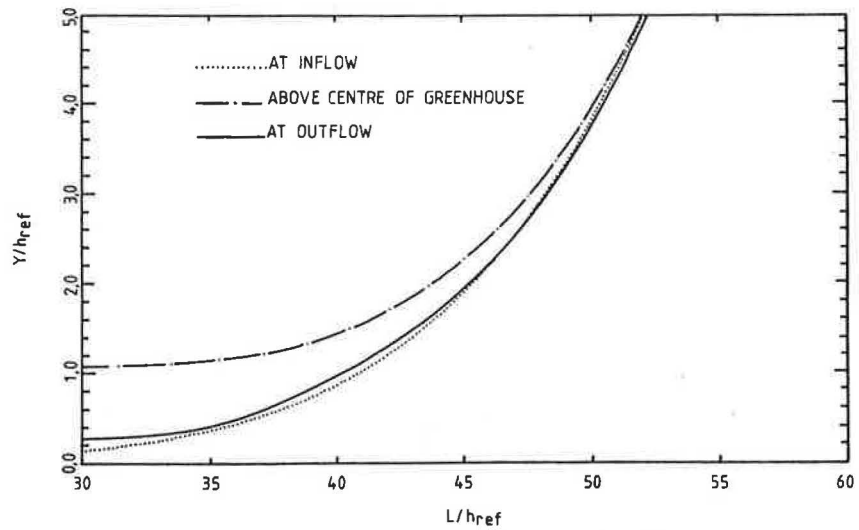


Fig. 6. Predicted non-dimensionalized turbulence length scales ($L/h_{ref}$) at different positions in the flow domain.

zero at the back of the greenhouse). The reason for this discrepancy could also be the deformation in the exterior profile of the greenhouse at high winds.

An important advantage of numerical modelling over measurements is that complete information of all the relevant variables are available over the whole flow domain. In Figs 4–6 for example, values for horizontal velocities, turbulence intensity and turbulence length scales at different positions in the flow domain are shown. Figure 4 clearly shows the extent of the greenhouse's influence on the surrounding flow field.

The work described in this paper could in future be extended to compute the effects of flow over parabolic sections through the greenhouse. This would give some indication of the preferred orientation with respect to the prevailing wind direction.

## 4. SUMMARY AND CONCLUSIONS

A brief outline of a computational procedure, which was used to compute the wind loads on a film clad, semicircular greenhouse, was presented. Some computational results were discussed. The accuracy of computed wind loading data was found to be sufficient for structural design purposes. It is concluded that for many flow situations, numerical models could offer an attractive alternative to windtunnel or full-scale tests.

## REFERENCES


1. R. P. Hoxey and G. M. Richardson, Measurements of wind loads on full-scale film plastic clad greenhouses. *J. Wind Eng. Ind. Aerodyn.* **16**, 57–83 (1984).
2. T. Hanson, D. M. Summers and C. B. Wilson, A three-dimensional simulation of wind flow around buildings. *Int. J. numer. Meth. Fluids* **6**, 113–127 (1986).
3. D. A. Wells and R. P. Hoxey, Measurements of wind loads on full-scale glasshouses. *J. Wind Eng. Ind. Aerodyn.* **6**, 139–167 (1980).
4. R. P. Hoxey and G. M. Richardson, Wind loads on film plastic greenhouses. *J. Wind Eng. Ind. Aerodyn.* **11**, 225–237 (1983).
5. E. H. Mathews, The prediction of natural ventilation in buildings. D.Eng. dissertation, University of Potchefstroom, RSA (1985).
6. C. F. Shieh and W. Frost, Application of a numerical model to wind energy conversion systems siting relative to two-dimensional terrain features. Fifth International Conference on Wind Engineering, Colorado State University, Fort Collins, Colorado, II, IX-5-1–IX-5-10 (July 1979).
7. J. Bittle and W. Frost, Atmospheric flow over two-dimensional bluff surface obstructions. NASA CR 2750 (1976).
8. P. K. Yeung and S. C. Kot, Computation of turbulent flows past arbitrary two-dimensional surface-mounted obstructions. *J. Wind Eng. Ind. Aerodyn.* **18**, 177–190 (1985).
9. T. Hanson, F. Smith, D. M. Summers and C. B. Wilson, Computer simulation of wind flow around buildings. *Computer Aided Design* **14**, 27–31 (1982).
10. T. Hanson, D. M. Summers and C. B. Wilson, Numerical modelling of wind flow over buildings in two dimensions. *Int. J. numer. Meth. Fluids* **4**, 25–41 (1984).
11. D. M. Summers, T. Hanson and C. B. Wilson, A random vortex simulation of wind-flow over a building. *Int. J. numer. Meth. Fluids* **5**, 849–871 (1985).
12. B. E. Launder and D. B. Spalding, *Mathematical Models of Turbulence*. Academic Press, London (1972).
13. C. Scruton, *An Introduction to Wind Effects on Structures*. Oxford University Press, Oxford (1981).
14. S. V. Patankar, *Numerical Heat Transfer and Fluid Flow*. McGraw-Hill, New York (1980).
15. E. H. Mathews, Two-dimensional steady-state temperature distributions in corners of arbitrary shape. *Bldg Envir.* **21**, 183–188.